



Article

Geochronology and Geological Implications of Paleoproterozoic Post-Collisional Monzogranitic Dykes in the Ne Jiao-Liao-Ji Belt, North China Craton

Yan Zhao ^{1,2,3} , Junchao Lyu ^{1,*}, Xu Han ⁴, Shoufa Lin ², Peng Zhang ^{1,3}, Xueming Yang ⁵  and Cong Chen ^{1,3}¹ Shenyang Centre, China Geological Survey, Shenyang 110034, China; zhaoyan@mail.cgs.gov.cn (Y.Z.)² Department of Earth and Environmental Sciences, University of Waterloo, Waterloo, ON N2L 3G1, Canada³ Key Laboratory of Deep Mineral Resources Exploration and Evaluation, Department of Natural Resource of Liaoning Province, Shenyang 110032, China⁴ School of Resources and Civil Engineering, Liaoning Institute of Science and Technology, Benxi 117004, China⁵ Manitoba Geological Survey, Winnipeg, MB R3C 0V8, Canada

* Correspondence: lvjunchao@mail.cgs.gov.cn

Abstract: Hardly any previous studies have focused on the granitic dykes which intrude into the Paleoproterozoic Liaohe Group in the Liaodong Peninsula, northeast of the North China Craton. In situ zircon U-Pb dating, Lu-Hf isotopic and geochemical analyses on three representative monzogranitic dykes were taken in this study. These dykes have relatively high content of SiO₂ (72.20%–74.78%) and K₂O (2.83%–6.37%), and have characteristics of high-K calc-alkaline to shoshonite series. Two dyke samples have I-type granite features and have high Sr/Y ratios and positive Eu anomalies, showing an adakitic feature. Another dyke has a high ratio of Ga/Al, but has a low Zr saturation temperature, which differs from the typical A-type granite. Zircon grains from these three dykes have typical magmatic zoning in CL images and yield consistent U-Pb ages of ~1859–1852 Ma, which are interpreted as the crystallization ages of these dykes. Hf isotopic analyses yield mainly negative ε_{Hf}(t) values and T_{DM2} ages of 2782–2430 Ma, similar to those of the 2.2–2.1 Ga granitoids and meta-sedimentary rocks (the Liaohe Group), indicating these monzogranitic dykes may have been sourced from melting of Paleoproterozoic granitoids and meta-sedimentary rocks. The monzogranitic dykes were generated under a post-collisional geological setting after the Jiao-Liao-Ji orogeny process.

Keywords: monzogranitic dykes; U-Pb zircon dating; Lu-Hf isotopes; post-collisional granites; Jiao-Liao-Ji Belt; North China Craton



Citation: Zhao, Y.; Lyu, J.; Han, X.; Lin, S.; Zhang, P.; Yang, X.; Chen, C. Geochronology and Geological Implications of Paleoproterozoic Post-Collisional Monzogranitic Dykes in the Ne Jiao-Liao-Ji Belt, North China Craton. *Minerals* **2023**, *13*, 928. <https://doi.org/10.3390/min13070928>

Academic Editor: Aleksei V. Travin

Received: 10 May 2023

Revised: 27 June 2023

Accepted: 4 July 2023

Published: 11 July 2023



Copyright: © 2023 by the authors. Licensee MDPI, Basel, Switzerland. This article is an open access article distributed under the terms and conditions of the Creative Commons Attribution (CC BY) license (<https://creativecommons.org/licenses/by/4.0/>).

1. Introduction

As one of the oldest cratons in the world, the North China Craton (NCC) is considered to be composed of the Eastern Block, the Western Block and Trans-North China Orogen [1,2]. Three major Paleoproterozoic orogenic belts have been recognized within the NCC [3], of which the Jiao-Liao-Ji Belt (JLJB) in the Eastern Block extends more than 1000 km ([4]; Figure 1). Great attention had been paid to the debate on the early Paleoproterozoic tectonic evolution model of the JLJB, and up to four tectonic models have been proposed as follows: an intra-continental rift opening and closing model [5,6], an arc-continent collision model [7–11], a rifting ocean followed by late subduction and collision model [6,12,13] and a back-arc basin (or retro-arc foreland basin) opening and closure model [14–17].

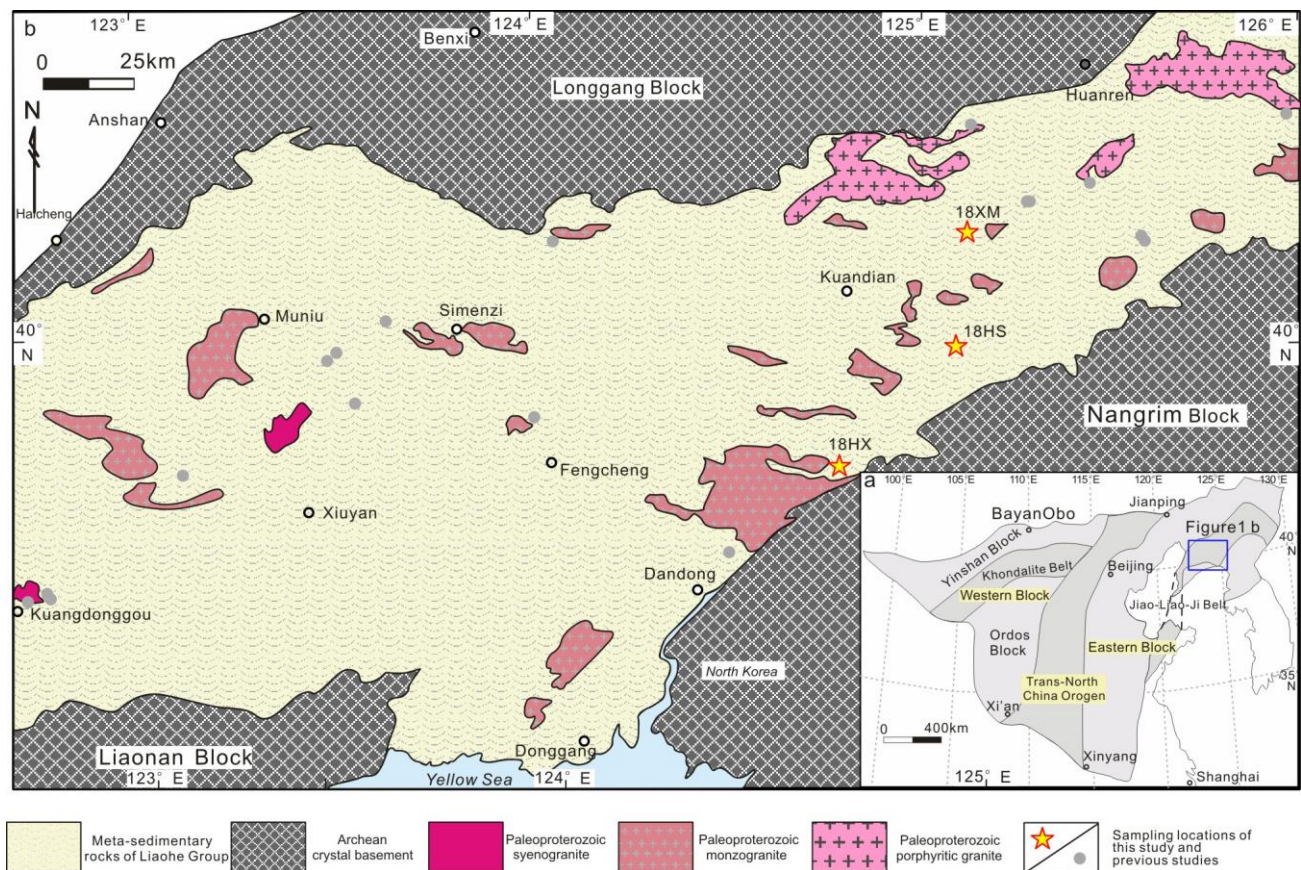


Figure 1. Simplified geological map of the Liaodong Peninsula (**b**) and part of the Jiao-Liao-Ji Belt in the North China Craton (**a**). (Modified after [18,19]). Locations of the monzogranitic dykes of this study are indicated.

Compared to the controversy regarding the early stage of its tectonic evolution, studies on the late Paleoproterozoic JLJB orogenic processes are not as well developed. Previous research has focused on the porphyritic granites [20], syenite [21,22], granitic leucosomes in granulites [23], metamorphic rocks [24] and pegmatite veins [25] from ~1880 Ma to 1860 Ma. The granitoids may have been distributed under a geological setting related to the JLJB complex and long-term evolution of the orogeny process. Although some granitoids are interpreted as originating under a post-collisional setting after the orogeny process, hardly any robust field evidence with corresponding geochronological evidence has been provided.

The Paleoproterozoic granitoid dykes, which were newly discovered during recent geological mapping fieldwork in the Liaodong Peninsula in Northeast China, enable us to better understand the post-collision process of the JLJB. Here, we report results of geochemical, zircon U-Pb ages, and Hf isotope studies of the three dykes in the Kuandian and Dandong areas (Figure 1), aiming to constrain the age and petrogenesis of post-collisional granites and to better understand the tectonic evolution process of the JLJB.

2. Geological Settings

The JLJB in the Eastern Block of the NCC is located between the Archean Longgang and the Liaonan-Nangrim blocks and extends into the Jiaodong Peninsula to the southwest (Figure 1a; [1,26,27]). Voluminous sedimentary rocks, granitoids, volcanic rocks and metamorphic rocks were involved in the intense orogenic process in ~1.9 Ga and experienced related deformation [28–33]. The Liaohe Group in the Liaoning Province is correlated with the Laoling and Ji'an groups in the Jilin Province and the Fenzishan and Jingshan groups in the Shandong Province. The Liaohe Group consists of meta-sedimentary

rocks and some meta-volcanic rocks and is subdivided into the Langzishan, Lieryu, Gaojiayu, Dashiqiao, and Gaixian formations [4,5,34]. Previous researchers summarized the widely distributed igneous rocks data and distinguished five magmatic episodes [20,21] as follows: ca. 2190–2160 Ma A2-type granites with minor basaltic dykes and tuffs, ca. 2160–2110 Ma tholeiitic rocks, ca. 2110–2080 Ma mafic rocks and aluminous A2-type granites, ca. 2010–1885 Ma adakitic granites related to regional metamorphism and ca. 1875–1850 Ma post-collisional granites.

Post-collisional granites are represented by the biotite-bearing and garnet-bearing porphyritic granites in the Kuandian and Huanren areas [20], syenite in the Kuangdonggou area [22], and quartz diorite in the Qinghe area [24]. These undeformed granitoids intruded into the deformed Paleoproterozoic meta-sedimentary rocks and early gneissic granitoids. In addition, hardly any reliable post-collisional contemporary mafic intrusion or dykes are reported at this period within the JLJB.

3. Sample Materials and Analytical Methods

3.1. Sample Materials

The granitic dykes from the Kuandian and Dandong areas, eastern Liaodong Peninsula, had a width of one to two meters and a length of tens of meters. Unlike the leucosomes in granulites and gneiss, which had a width of a few centimeters and paralleled the foliation of granulites as [23] reported, these granitic dykes are observed to intrude into the Paleoproterozoic Gaixian and Gaojiayu formations either cutting through or following the foliation of gneiss (Figure 2).

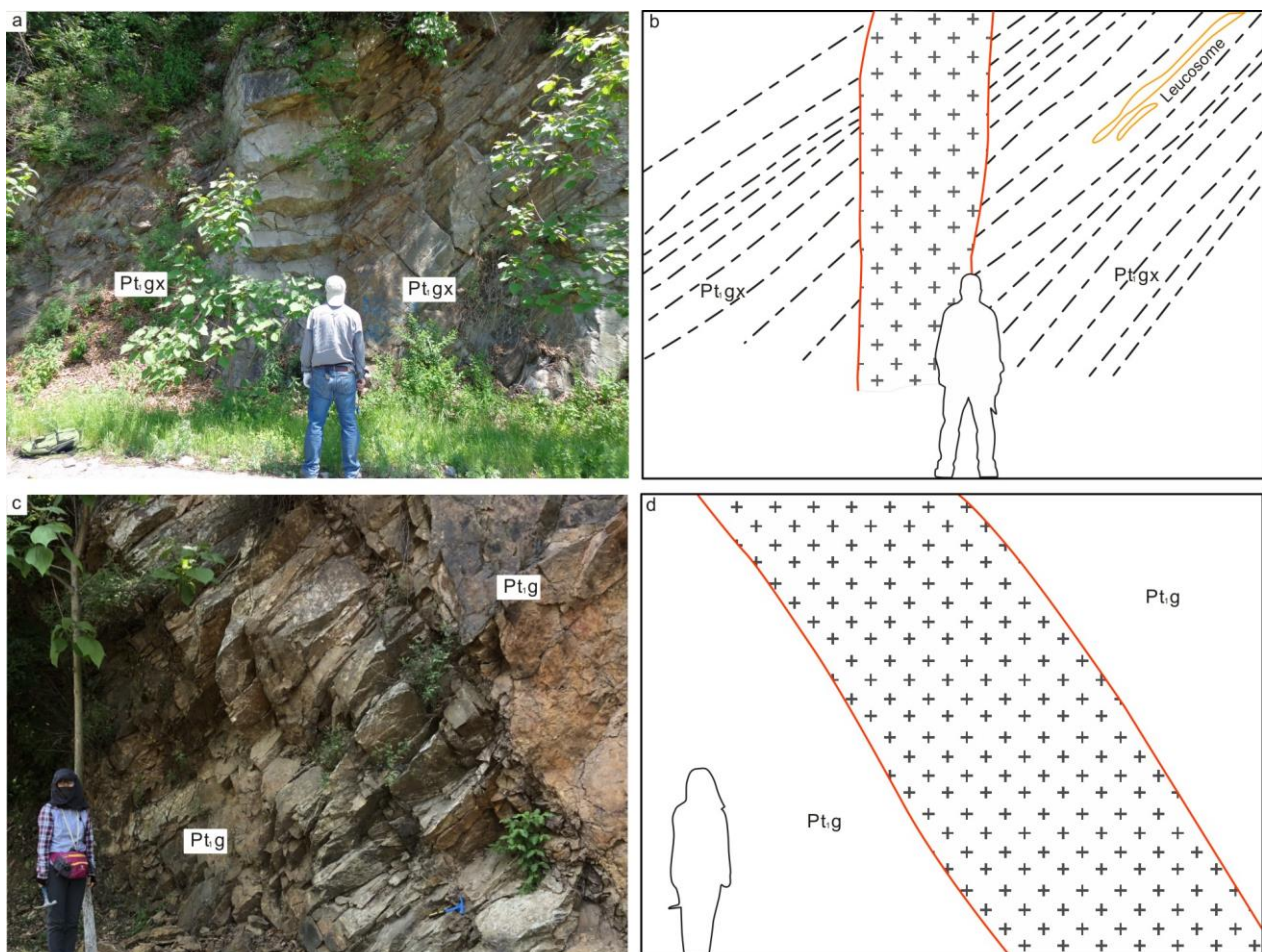


Figure 2. Cont.

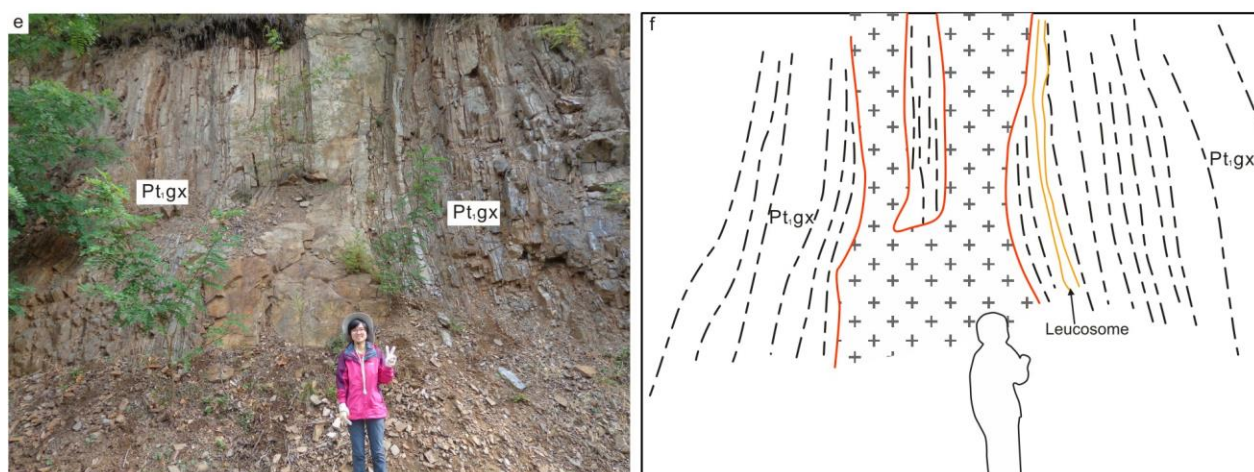


Figure 2. Field photographs and sketches of the studied monzogranitic dykes in the Kuandian and Dandong areas within the Jiao-Liao-Ji Belt: (a,b) sample 18XM, (c,d) sample 18HX, (e,f) sample 18HS ((a): a monzogranitic dyke intrudes into the Paleoproterozoic Gaixian Formation gneiss and cuts the foliation of the gneiss near Kuandian County; (c): a monzogranitic dyke intrudes into the Paleoproterozoic Gaojiayu Formation granulite in the Hushan area; (e): a granitic dyke intrudes into the Gaixian Formation schist and gneiss near the Hongshi area) Pt₁g: Paleoproterozoic Gaojiayu Formation granulite; Pt₁gs: Paleoproterozoic Gaixian Formation schist and gneiss.

Sample 18XM (40°53'11" N, 125°8'40" E) was collected from a 1 m wide monzogranite dyke that intrudes into the Gaixian Formation schist and gneiss (Figure 2a). Sample 18HX (40°22'41" N, 124°43'40" E) was collected from a 2 m wide dyke that intrudes into the Gaojiayu Formation granulite near Hushan Town (Figure 2c). Sample 18HS is a coarse-grained granite (40°41'00" N, 125°9'01" E) collected from a 1.5 m wide dyke that intrudes into the Gaixian Formation schist and gneiss near Hongshi Town (Figure 2e).

3.2. Thin Section Petrography

The thin sections of the studied granitoids were prepared for optical petrography at the Shenyang Institute of Geology and Mineral Resources, Shenyang, China. Small pieces of rock were cut from the field samples with a diamond blade, and then mounted on a petrography carrier glass (~27 mm × 47 mm). The mounted sections were polished by using a range of ever-finer abrasive powders down to a thickness of 50 μm. Based on the polished thin sections, the microstructure, texture and mineral modal contents in vol% were estimated by point counting using an optical petrography microscope in both transmitted and polarized light.

3.3. Major and Trace Elements

After removal of altered surfaces, fresh whole-rock samples were crushed and ground to 200 mesh size in an agate mill. Chemical analyses were conducted at the Shenyang Institute of Geology and Mineral Resources, Shenyang, China. X-ray fluorescence (XRF, PANALYTICAL, Almelo, Holland) (AXIOS-Minerals) using fused glass disks and inductively coupled plasma mass spectrometry (ICP-MS, Agilent company, Santa Clara, CA, USA) (Agilent 7500a with a shield torch) were used to measure major and trace element compositions, respectively. The detailed sample-digesting procedure is as follows: Sample powder (200 mesh) was placed in an oven at 105 °C and dried for 12 h, then ~1.0 g dried sample was accurately weighted and placed in the ceramic crucible and then heated in a muffle furnace at 1000 °C for 2 h. After cooling to 400 °C, this sample was placed in the drying vessel and weighted again in order to calculate the loss on ignition (LOI). Sample powder (0.6 g) was mixed with 6.0 g cosolvent (Li₂B₄O₇:LiBO₂:LiF = 9:2:1) and 0.3 g oxidant (NH₄NO₃) in a Pt crucible, which was placed in the furnace at 1150 °C for 14 min. Then, this melting sample was quenched with air for 1 min to produce flat discs on the fire brick

for the XRF analyses. Fe_2O_3 and FeO content were measured directly, while the FeO^{T} was calculated (Supplementary Table S1). The detection limit of XRF differs from 0.001% to 1% following GB/T 14506.1-2010 standard. For trace element analysis, (1) 50 mg sample powder was accurately weighed and placed in a Teflon bomb; (2) 1 mL HNO_3 and 1 mL HF were slowly added into the Teflon bomb; (3) Teflon bomb was placed in a stainless steel pressure jacket and heated to 190 °C in an oven for >24 h; (4) after cooling, the Teflon bomb was opened and placed on a hotplate at 140 °C and evaporated to incipient dryness, and then 1 mL HNO_3 was added and evaporated to dryness again; (5) 1 mL of HNO_3 , 1 mL of MQ water and 1 mL internal standard solution of 1 ppm In were added, and the Teflon bomb was resealed and placed in the oven at 190 °C for >12 h; (6) the final solution was transferred to a polyethylene bottle and diluted to 100 g by the addition of 2% HNO_3 . Precision and accuracy were better than 5% for major elements and 10% for trace elements based on repeated analyses of the USGS standards BHVO-1, BCR-2, and AGV-1 [35]. The detection limit of ICP-MS differed from 0.003 to 1×10^{-6} following GB/T 14506.30-2010 standard.

3.4. Zircon LA-ICP-MS U-Pb Dating

Zircon grains from the granitoid samples were extracted using heavy-liquid and magnetic separation, and purified by hand-picking under a binocular microscope. Zircons were mounted and polished before cathodoluminescent (CL) images were taken to examine the internal structure and potential inclusions of individual grains. U-Pb dating and trace element analysis of zircon were simultaneously conducted by LA-ICP-MS (Agilent company, Santa Clara, CA, USA) (Agilent 7700e) at the Wuhan Sample Solution Analytical Technology Co., Ltd., Wuhan, China. Laser sampling was performed using a GeolasPro laser ablation system that consists of a COMPexPro 102 ArF excimer laser (wavelength of 193 nm and maximum energy of 200 mJ) and a MicroLas optical system. Helium was applied as a carrier gas. Argon was used as the make-up gas and was mixed with the carrier gas via a T-connector before entering the ICP system. The laser beam diameter was 35 μm and the repetition rate was 5 Hz. Each spot analysis consisted of a ~5 s background measurement and a 45 s sample measurement. The $^{207}\text{Pb}/^{206}\text{Pb}$, $^{206}\text{Pb}/^{238}\text{U}$, $^{207}\text{Pb}/^{235}\text{U}$ and $^{208}\text{Pb}/^{232}\text{Th}$ values were corrected for instrumental isotopic and elemental fractionation effects using zircon standard 91500. An Excel-based software, ICPMSDataCal (ICPMSdatacal Excel2016, Redmond, WA, USA), was used to perform off-line selection and integration of the background. It also analyzed signals, time-drift correction and quantitative calibration for trace element analysis and U-Pb dating [36]. Concordia diagrams and weighted mean calculations were made using Isoplot/Ex_ver3 (Ludwig, Berkeley, CA, USA) [37].

3.5. Zircon Lu-Hf Ratio Analyses

The in situ Lu-Hf isotope analyses ($n = 42$) were also conducted by MC-ICP-MS at the Wuhan Sample Solution Analytical Technology Co., Ltd. (Wuhan, China). A stationary spot used a beam diameter of ~55 μm . Helium was used to transport the ablated sample aerosol mixed with argon from the laser-ablation cell to the MC-ICP-MS torch by a mixing chamber. $^{176}\text{Lu}/^{175}\text{Lu} = 0.02658$ and $^{176}\text{Yb}/^{173}\text{Yb} = 0.796218$ ratios were determined to correct for the isobaric interferences of ^{176}Lu and ^{176}Yb on ^{176}Hf [38]. The $^{176}\text{Hf}/^{177}\text{Hf}$ and $^{176}\text{Lu}/^{177}\text{Hf}$ ratios of the 91500 standard zircon were 0.282270 ± 0.000023 (2σ , $n = 15$) and 0.00028, similar to the commonly accepted $^{176}\text{Hf}/^{177}\text{Hf}$ ratio of 0.282284 ± 0.000003 (1σ) measured using the solution method [39]. Zircon international standard GJ-1 was used as the reference standard, with a weighted mean $^{176}\text{Hf}/^{177}\text{Hf}$ ratio of 0.282006 ± 32 (2SD, $n = 24$).

4. Results

4.1. Petrography

The 18XM sample has a fine- to medium-grained texture and a grey to light-brown color (Figure 3a,b). Minerals in the monzogranite include quartz (~30 vol%), plagioclase

(~30 vol%), orthoclase (~35 vol%) and biotite (<5 vol%). The 18HX sample has a characteristic medium-grained texture and a grey color (Figure 3c). Quartz (~30 vol%), plagioclase (~33 vol%), orthoclase (~25 vol%), biotite (~10 vol%) and minor muscovite (~2 vol%) comprise the minerals in this monzogranite. The 18HS sample has a characteristic coarse-grained texture and a grey to brown color (Figure 3d). Plagioclase (~40 vol%), orthoclase (~35 vol%), quartz (~23 vol%) and minor biotite (~2 vol%) comprise this monzogranite.

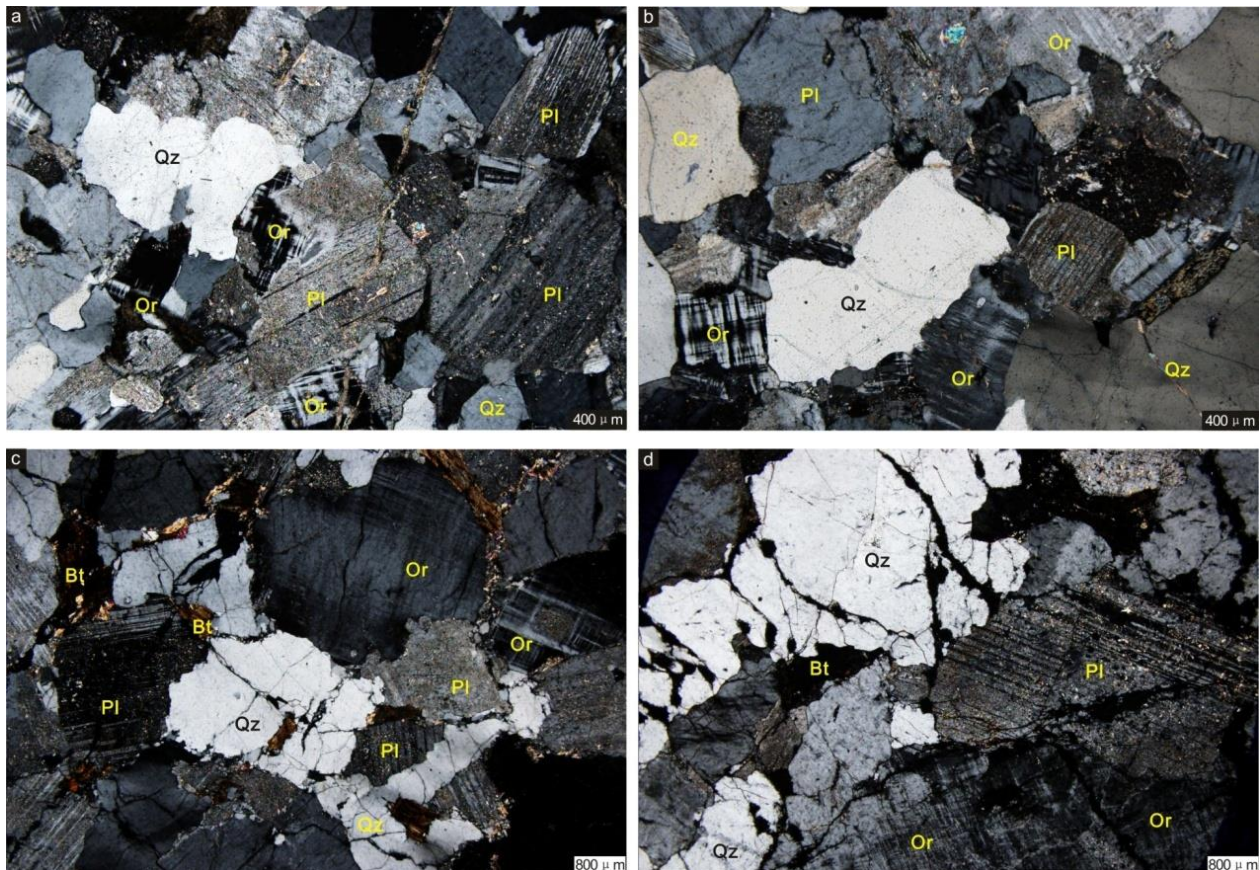


Figure 3. Photomicrographs of the studied monzogranitic dykes in the Kuandian and Dandong areas (images are without analysator). (a,b) Sample 18XM, (c) sample 18HX, (d) sample 18HS (Bt: biotite; Or: orthoclase; Pl: plagioclase; Qz: quartz).

4.2. Major and Trace Elements

The 18XM samples have a relatively high content of SiO_2 (72.81–74.78 wt%) and K_2O (5.52–5.70 wt%), and plot into the metaluminous and peraluminous field (Figure 4b). The 18HS and 18HX granitic dyke samples also have a relatively high content of SiO_2 (72.20–74.08 wt%) and K_2O (2.83–6.37 wt%) and plot into the fields of high-K calc-alkaline to shoshonite series. These two samples have medium Al_2O_3 contents, and in the A/NK versus A/CNK diagram they are mainly metaluminous to weakly peraluminous (Figure 4b). Major and trace element content of the three analyzed granitoid dykes are given in Supplementary Table S1 and Figure 5. The 18HS and 18HX samples exhibit similar chondrite-normalized rare earth element (REE) patterns with marked positive Eu anomalies ($\text{Eu}/\text{Eu}^* = 2.16\text{--}4.70$). The 18XM samples are also enriched in light REE but with strong negative Eu anomalies ($\text{Eu}/\text{Eu}^* = 0.31\text{--}0.53$).

4.3. Zircon U-Pb Geochronology

CL images of representative zircons from the three samples are listed in Supplementary Table S2 and Figure 6. Zircon grains have similar euhedral to subhedral shape and are

about 70 to 200 μm long. Th/U ratios of the testing grains range from 0.11 to 0.86, indicating an igneous origin. Fifteen spots from sample 18XM and thirty spots from sample 18HS are analyzed, yielding intercept U-Pb age of 1859 ± 33 Ma (MSWD = 2.1) and 1852 ± 10 Ma (MSWD = 1.02), respectively. Twenty-five spots from sample 18HX yield weighted mean $^{207}\text{Pb}/^{206}\text{Pb}$ ages of 1856 ± 12 Ma (MSWD = 1.3) (Figure 6).

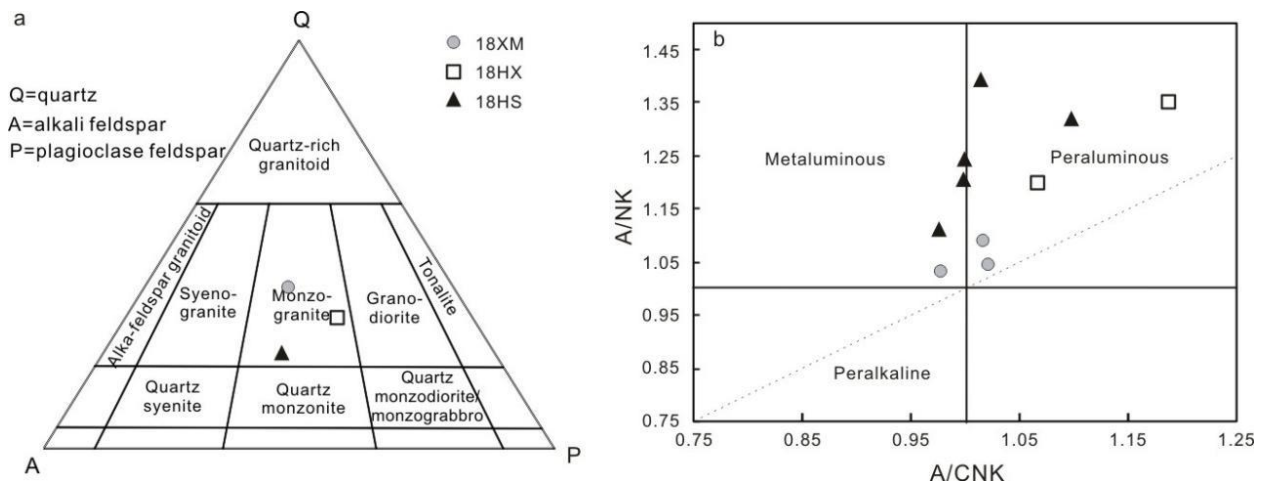


Figure 4. Discrimination diagrams for the monzogranitic dykes in the Jiao-Liao-Ji Belt. (a) Quartz-alkali feldspar-plagioclase feldspar classification diagram (after [40]); (b) A/CNK versus A/NK after Maniar and Piccoli [41].

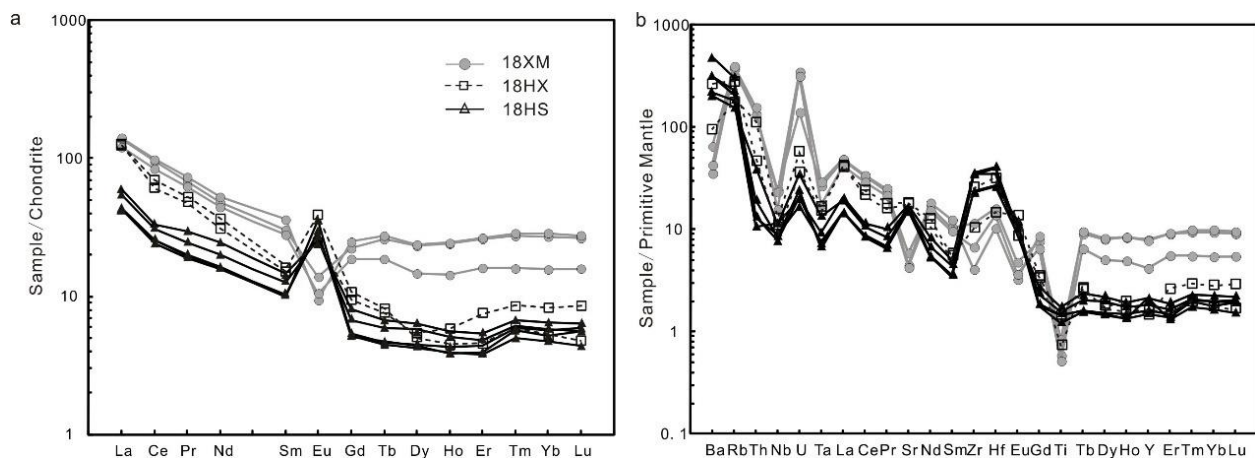


Figure 5. CI chondrite-normalized REE (a) and primitive mantle-normalized trace elements distribution (b) patterns for the monzogranitic dykes in the Jiao-Liao-Ji Belt (CI chondrite and primitive mantle values are from [42]).

4.4. Zircon Lu-Hf Isotopic Characteristics

Zircon analytical spots with concordant U-Pb ages are analyzed for their Lu-Hf isotope contents. Results are listed in Supplementary Table S3 and Figure 7. Sample 18HX yielded negative $\varepsilon_{\text{Hf}}(t)$ values, ranging between -4.0 and -0.9 . The initial $^{176}\text{Hf}/^{177}\text{Hf}$ ratios ranged from 0.281482 to 0.281607, with calculated T_{DM1} ages of 2447–2302 Ma and T_{DM2} ages of 2782–2566 Ma. Sample 18XM also yielded negative $\varepsilon_{\text{Hf}}(t)$ values, ranging between -2.8 and -6.8 . The initial $^{176}\text{Hf}/^{177}\text{Hf}$ ratios ranged from 0.281484 to 0.281540, with calculated T_{DM1} ages of 2377–2452 Ma and T_{DM2} ages of 2696–2826 Ma. Similarly, initial $^{176}\text{Hf}/^{177}\text{Hf}$ ratios of zircons from 18HS were from 0.281573 to 0.281669, with calculated T_{DM1} ages of 2338–2206 Ma and T_{DM2} ages of 2640–2430 Ma. The $\varepsilon_{\text{Hf}}(t)$ values for 18HS ranged from -2.5 and $+1.2$.

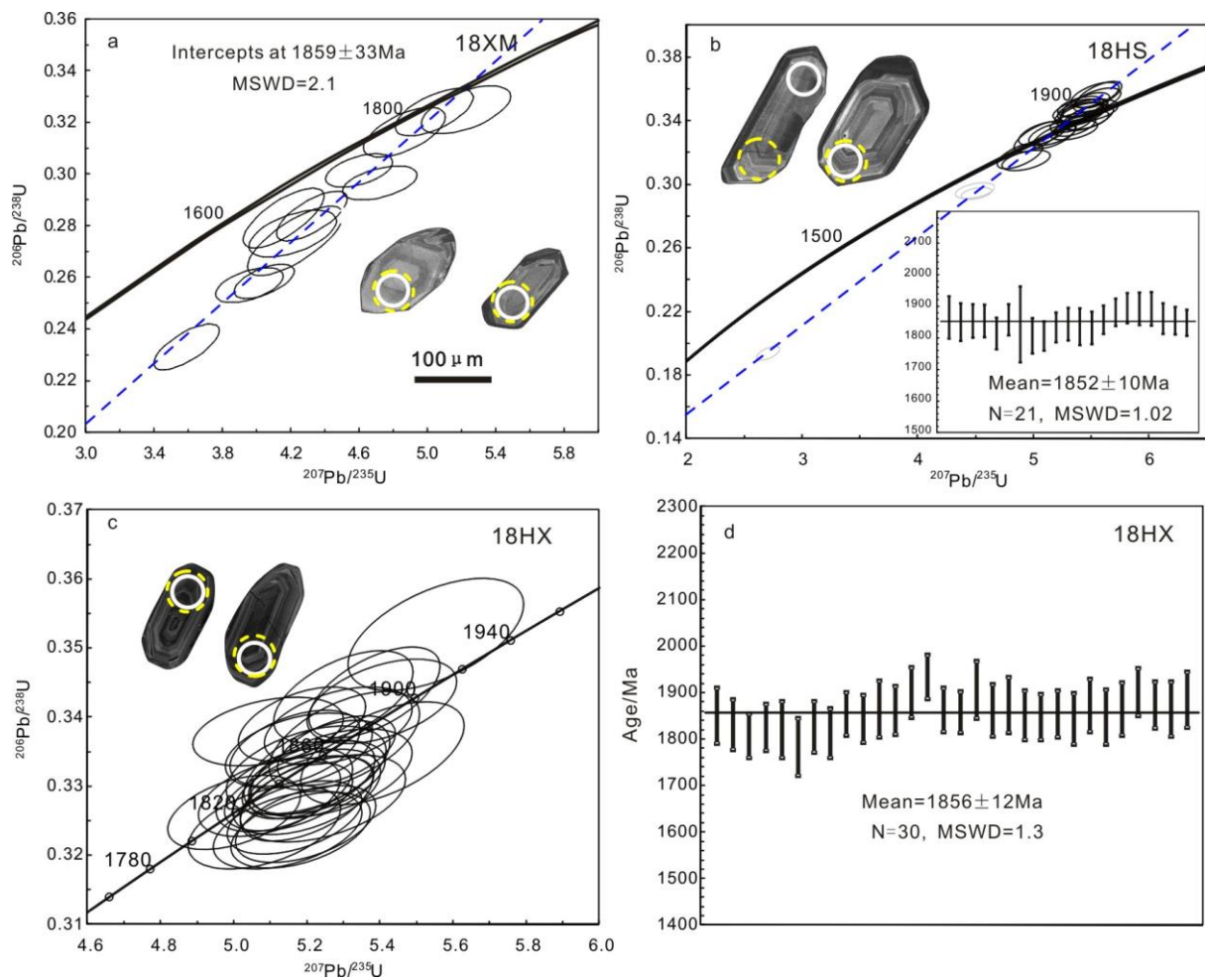


Figure 6. Concordia diagrams for U-Pb analyses of zircons from monzogranitic dykes in the Jiao-Liao-Ji Belt, the 35- μm analytical spots of U-Pb (white ring) and 50 μm analytical spots of Hf (yellow ring) analysis of represented zircon grains are also shown. Respective error range (ellipse and bar) of 2SD is shown. (a) Sample 18XM; (b) sample 18HS; (c,d) sample 18HX.

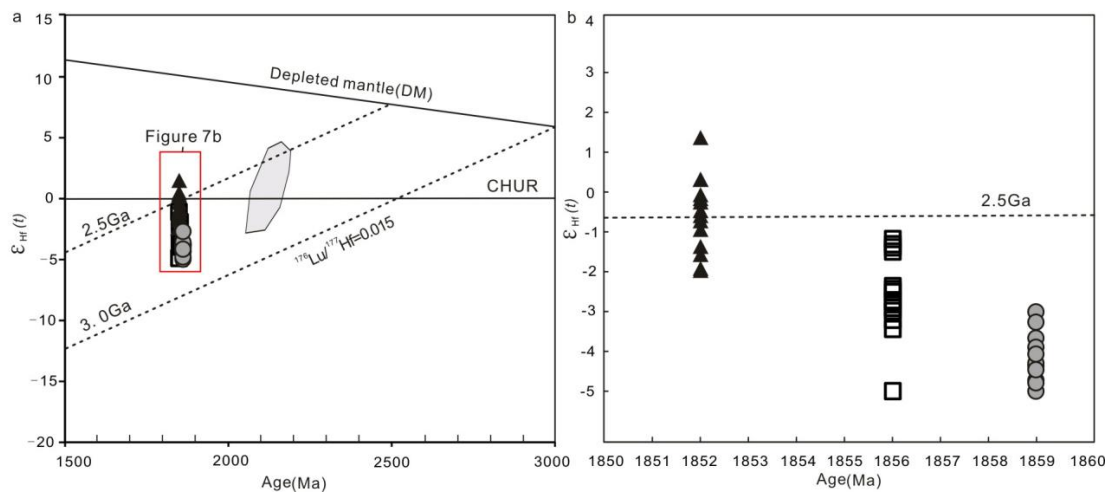


Figure 7. Zircon $^{207}\text{Pb}/^{206}\text{Pb}$ ages versus $\epsilon_{\text{Hf}}(t)$ values of the monzogranitic dykes in the Jiao-Liao-Ji Belt (a,b). Lu-Hf evolution line for depleted mantle is constrained by a present-day $^{176}\text{Hf}/^{177}\text{Hf}$ ratio of 0.28325 [43] and $^{176}\text{Lu}/^{177}\text{Hf}$ ratio of 0.0384 [38]. The gray polygon is the Paleoproterozoic Hf isotopic data from [20]. Legend is similar with that in Figure 5.

5. Discussion

5.1. U-Pb Ages of the Monzogranitic Dykes and the Granitoids Geochronology within the JLJB

Three monzogranitic dykes were observed cutting through foliation of the deformed Liaohe Group meta-sedimentary rocks during the fieldwork (Figure 2). Zircon grains from these dykes exhibit typical oscillatory zoning in CL images, with most Th/U ratios greater than 0.2, indicating a magmatic origin [44]. These zircon grains yield consistent U-Pb ages of ~1859 to 1852 Ma (Supplementary Table S2, Figure 6), showing that these monzogranitic dykes crystallized ~1860–1850 Ma.

Previous researchers have summarized igneous rocks and their relations with the tectonic evolution process of the JLJB, and established different evolution stages [4,18,19]. Here, we also list Late Paleoproterozoic granitoids types and available ages in Liaoning and Jilin provinces in Table 1. Taking these studies into consideration, three stages of granitoids could be recognized as follows. An early magmatic event of ~2200 to 2140 Ma, indicated by A-type and I-type granites, which are also known as the Liaoji Granites [26,45–47]. A middle period consisting of ~1890 to 1860 Ma biotite-bearing and garnet-bearing porphyritic granites, pegmatite and adakitic granites. They were believed to be accompanied by peak metamorphism in the JLJB [16,25,33] or by Paleoproterozoic oceanic slab subduction [48]. A post-collisional magmatic event at ~1855 to 1840 Ma, is represented by the monzogranite dykes in this study, syenite in the Kuangdonggou area, and sporadically pegmatite dykes [21,25].

Table 1. Geological characteristics and chronological results of Late Paleoproterozoic granites in the Liao-Ji region.

Intrusion Location	Location/GPS	Lithology	Methods	Testing Spots	Age/Ma	Interpretation	Reference
Sanjiazi	40°44'22" N 123°15'32" E	Pegmatite	LA ICP-MS	30	1814 ± 20 Ma	Crystallization age	[25]
Sanjiazi	40°51'11" N 123°19'27" E	Pegmatite	LA ICP-MS	26	1869 ± 22 Ma	Crystallization age	[25]
Sanjiazi	40°42'06" N 123°13'30" E	Pegmatite	LA ICP-MS	37	1873 ± 17 Ma	Crystallization age	[25]
Yangmugan	40°38'16" N 125°07'20" E	Pegmatite	LA ICP-MS	41	1842 ± 7 Ma	Crystallization age	[25]
Yangmugan	40°38'01" N 125°07'43" E	Pegmatite	LA ICP-MS	30	1866 ± 13 Ma	Crystallization age	[25]
Xiaomiao Dyke	40°53'11" N 125°08'40" E	Monzogranite	LA ICP-MS	15	1859 ± 33 Ma	Crystallization age	This paper
Hongshi Dyke	40°22'41" N, 124°43'40" E	Monzogranite	LA ICP-MS	30	1852 ± 10 Ma	Crystallization age	This paper
Hushan Dyke	40°41'00" N, 125°9'01" E	Monzogranite	LA ICP-MS	29	1856 ± 12 Ma	Crystallization age	This paper
Dadingzi	Eastern Qingchengzi Town, Dandong City	Monzogranite	SIMS	12	1869 ± 16 Ma	Crystallization age	[49]
Nantaizi	40°31'42" N, 122°48'37" E	Monzogranite	LA ICP-MS	31	1851 ± 11 Ma	Crystallization age	[50]
Housongshu	40°28'12" N, 122°56'12" E	Trondhjemite	LA ICP-MS	16	1892 ± 16 Ma	Crystallization age	[50]
Taipingshao	10 km north of Taipingshao Town Dandong City	Granite	LA ICP-MS	28	1892 ± 38 Ma	Crystallization age	[51]
Taipingshao	12 km north of Taipingshao Town Dandong City	Granite	LA ICP-MS	27	1859 ± 36 Ma	Crystallization age	[51]
Kuangdonggou	Kuangdonggou Town Gaizhou City	Syenite	LA ICP-MS	19	1879 ± 17 Ma	Crystallization age	[22]
Kuangdonggou	Kuangdonggou Town Gaizhou City	Syenite	LA ICP-MS	17	1874 ± 18 Ma	Crystallization age	[22]
Kuangdonggou	5 km west of Kuangdonggou Town Gaizhou City	Diorite	LA ICP-MS	12	1870 ± 18 Ma	Crystallization age	[22]
Sizhanggunzi	Sizhanggunzi village Gaizhou City	Granodiorite	LA ICP-MS	19	1871.2 ± 9.3 Ma	Crystallization age	[52]
Qinghe	Qianjin Village Qinghe Town Ji'an City	Quartz diorite	SIMS	12	1877 ± 15 Ma	Crystallization age	[21]

Table 1. Cont.

Intrusion Location	Location/GPS	Lithology	Methods	Testing Spots	Age/Ma	Interpretation	Reference
Shuangcha	Shuangcha Village Ji'an City	Garnet-bearing porphyritic granite	LA ICP-MS	30	1890 ± 21 Ma	Crystallization age	[53]
Wuleishan	Northwest of Sanjiazi Town Anshan City	Porphyritic granite	SIMS	12	1830.5 ± 5.9 Ma	Crystallization age	[49]
Shuangcha	Huangweizi Village Ji'an City	porphyritic biotite mozogranite	SIMS	17	1872 ± 9 Ma	Crystallization age	[21]
Shuangcha	Zhongxing Village Ji'an City	Rapakivi granite	SIMS	18	1867 ± 13 Ma	Crystallization age	[21]
Lujiapuzi	Pulepu Town Fushun City	Rapakivi granite	SIMS	19	1847 ± 40 Ma	Crystallization age	[21]
13th Gou	13th Gou Baishan City Jilin Province	Garnet-bearing porphyritic granite	LA ICP-MS	20 11	1868 ± 9 Ma 1848 ± 13 Ma	Crystallization age, Metamorphic age	[20]
12th Gou	12th Gou Baishan City Jilin Province	Garnet-bearing porphyritic granite	LA ICP-MS	42 9	1872 ± 6 Ma 1851 ± 14 Ma	Crystallization age, Metamorphic age	[20]
Huadian	Huadian Town Ji'an City Jilin Province	Garnet-bearing porphyritic granite	LA ICP-MS	26 13	1871 ± 7 Ma 1850 ± 12 Ma	Crystallization age, Metamorphic age	[20]
Huadian	Huadian Town Ji'an City Jilin Province	Garnet-bearing porphyritic granite	LA ICP-MS	26 10	1866 ± 2 Ma 1850 ± 4 Ma	Crystallization age, Metamorphic age	[20]
Huadian	Taishang Town Ji'an City Jilin Province	Garnet-bearing porphyritic granite	LA ICP-MS	35 11	1869 ± 2 Ma 1850 ± 4 Ma	Crystallization age, Metamorphic age	[20]
Laoheishan	Laoheishan Village Dandong City Liaoning Province	Garnet-bearing porphyritic granite	LA ICP-MS	25 11	1872 ± 8 Ma 1851 ± 12 Ma	Crystallization age, Metamorphic age	[20]
Jiguanshan	Jiguanshan Town Dandong City Liaoning Province	Garnet-bearing porphyritic granite	LA ICP-MS	31 13	1870 ± 7 Ma 1850 ± 11 Ma	Crystallization age, Metamorphic age	[20]
Laoheishan	Laoheishan Village Dandong City Liaoning Province	Garnet-bearing porphyritic granite	LA ICP-MS	27 11	1868 ± 3 Ma 1846 ± 5 Ma	Crystallization age, Metamorphic age	[20]
Jiguanshan	Jiguanshan Town Dandong City Liaoning Province	Garnet-bearing porphyritic granite	LA ICP-MS	25 12	1870 ± 3 Ma 1842 ± 4 Ma	Crystallization age, Metamorphic age	[20]
12th Gou	12th Gou Baishan City Jilin Province	Biotite-bearing porphyritic granite	LA ICP-MS	34 8	1868 ± 6 Ma 1849 ± 13 Ma	Crystallization age, Metamorphic age	[20]
11th Gou	11th Gou Baishan City Jilin Province	Biotite-bearing porphyritic granite	LA ICP-MS	20 14	1872 ± 7 Ma 1849 ± 9 Ma	Crystallization age, Metamorphic age	[20]
Qinghe	Qinghe Town Ji'an City Jilin Province	Biotite-bearing porphyritic granite	LA ICP-MS	24 19	1865 ± 7 Ma 1849 ± 9 Ma	Crystallization age, Metamorphic age	[20]
Sipingxiang	Sipingxiang Fushun City Liaoning Province	Biotite-bearing porphyritic granite	LA ICP-MS	28 10	1872 ± 7 Ma 1850 ± 13 Ma	Crystallization age, Metamorphic age	[20]
Taipingshao	West of Taipingshao Town Dandong City Liaoning Province	Biotite-bearing porphyritic granite	LA ICP-MS	17 11	1867 ± 10 Ma 1842 ± 12 Ma	Crystallization age, Metamorphic age	[20]
Yahe	East of Yahe Town Dandong City Liaoning Province	Biotite-bearing porphyritic granite	LA ICP-MS	33 16	1865 ± 6 Ma 1849 ± 8 Ma	Crystallization age, Metamorphic age	[20]
Gulouzi	North of Gulouzi Town Dandong City Liaoning Province	Biotite-bearing porphyritic granite	LA ICP-MS	18 14	1864 ± 8 Ma 1844 ± 9 Ma	Crystallization age, Metamorphic age	[20]
11th Gou	11th Gou Baishan City Jilin Province	Biotite-bearing porphyritic granite	LA ICP-MS	28 11	1864 ± 2 Ma 1846 ± 4 Ma	Crystallization age, Metamorphic age	[20]

Table 1. Cont.

Intrusion Location	Location/GPS	Lithology	Methods	Testing Spots	Age/Ma	Interpretation	Reference
Qinghe	Qinghe Town Ji'an City Jilin Province	Biotite-bearing porphyritic granite	LA ICP-MS	40 27	1867 ± 2 Ma 1847 ± 3 Ma	Crystallization age, Metamorphic age	[20]
Taipingshao	West of Taipingshao Town Dandong City Liaoning Province	Biotite-bearing porphyritic granite	LA ICP-MS	38 14	1869 ± 3 Ma 1849 ± 3 Ma	Crystallization age, Metamorphic age	[20]
11th Gou	11th Gou Baishan City Jilin Province	Flesh-red porphyritic granite	LA ICP-MS	30 24	1868 ± 8 Ma 1849 ± 8 Ma	Crystallization age, Metamorphic age	[20]
Taipingshao	West of Taipingshao Town Dandong City Liaoning Province	Flesh-red porphyritic granite	LA ICP-MS	39 8	1866 ± 6 Ma 1846 ± 13 Ma	Crystallization age, Metamorphic age	[20]

5.2. Genesis of the Monzogranitic Dykes

The monzogranite dykes in this study have a similar high SiO₂ content and alkalis and have low content of MgO, FeO^T and CaO (Supplementary Table S1). In the primitive mantle-normalized trace element diagram (Figure 5b), the 18HS and 18HX samples are enriched in large ion lithosphere elements (LILEs) with positive Eu (Figure 5a) and Ba, U anomalies and depleted in some high field-strength elements (HFSEs). The 18HS and 18HX samples also exhibit high Sr/Y ratio, indicating an adakitic granite feature (Figure 8a). The 18XM samples show relatively high content of U and HREE, but exhibit similar overall trace elements to those in 18HS and 18HX. The 18 XM samples have A-type granite features as their high ratios of Ga/Al, while the 18 HS and 18 HX samples show I-type granite characteristics (Figure 9). Further Zr saturation calculation results reveal that 18XM samples have the lowest temperature of 688 °C to 770 °C (Supplementary Table S1), rather than the high temperature of typical A-type granites [54–57]. Considering the distribution of the studied monzogranitic dykes within the JLJB, they should have been generated under a thickened crust tectonic setting.

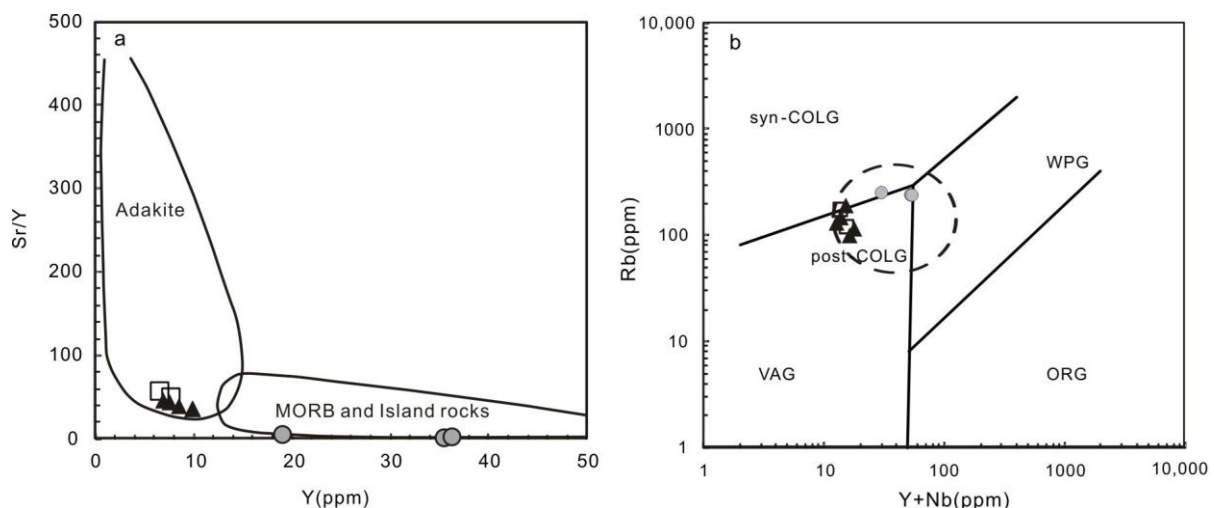


Figure 8. Sr/Y vs. Y diagram for the monzogranitic dykes in the Jiao-Liao-Ji Belt (a, after [58] and Rb-(Y + Nb) diagrams (b, after [59,60]). The circle in Figure 8a represents a post-collisional geodynamic setting of Pearce et al. [60] (MORB: mid ocean ridge basalt; ORG: orogenic granite; syn-COLG: syn-collisional granite; COLG: collisional granitoids; OA: oceanic arc; VAG: volcanic arc granite; WPG: within-plate granite). Legend is similar to that in Figure 5.

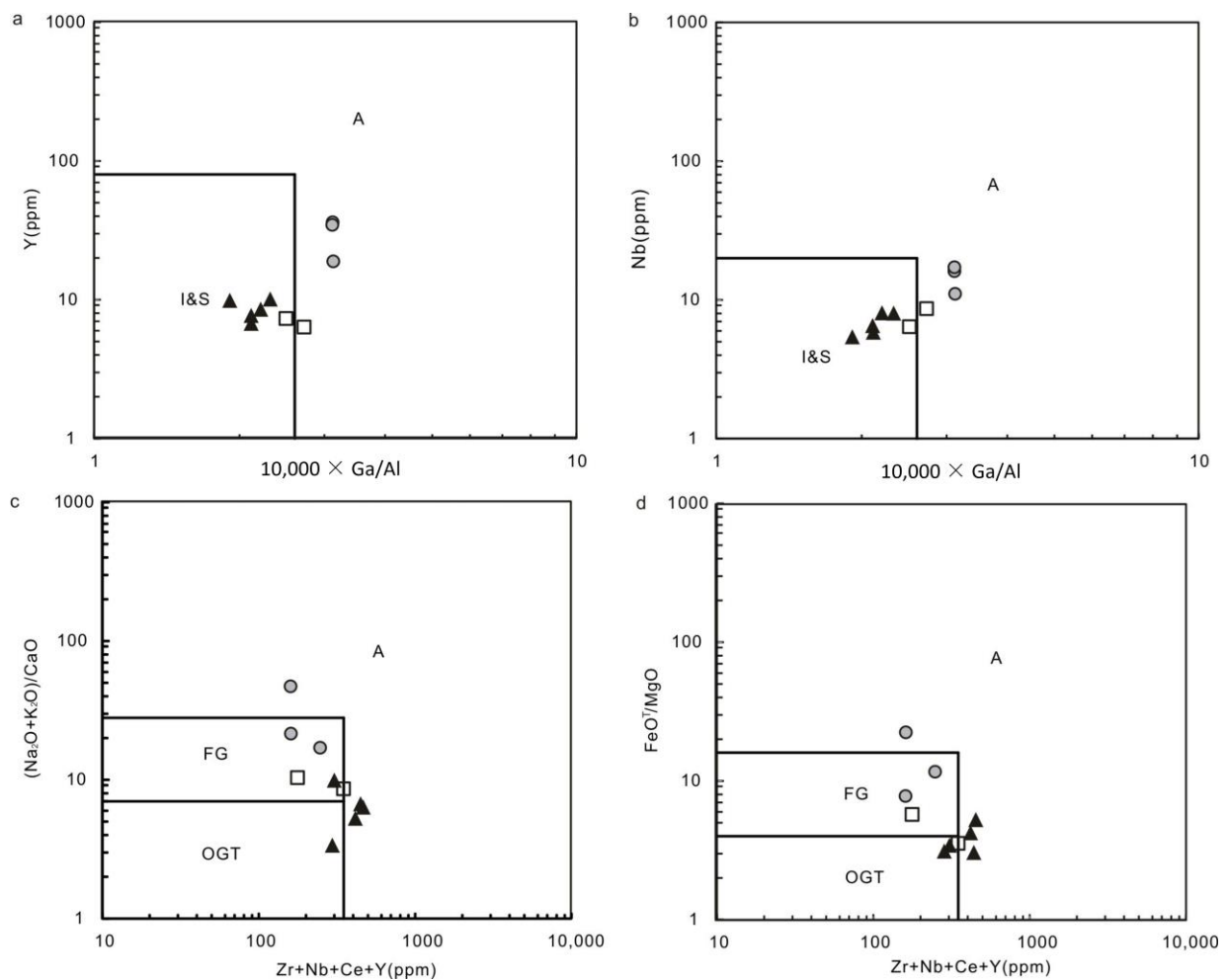


Figure 9. Y (a), Nb (b) versus $10,000 \times \text{Ga}/\text{Al}$ plots and $(\text{Na}_2\text{O} + \text{K}_2\text{O})/\text{CaO}$ (c), $\text{FeO}^{\text{T}}/\text{MgO}$ (d) versus $\text{Zr} + \text{Nb} + \text{Ce} + \text{Y}$ plots (after [54]) A, I and S = A-, I- and S-type granites, respectively; FG = fractionated felsic granites; OGT = unfractionated M-, I- and S-type granites, legend is similar to that in Figure 5.

Hf isotope analysis also illustrated similar conclusions. Hf isotope data show T_{DM2} ages of 2640–2430 Ma, and reveal that most of the negative $\varepsilon_{\text{Hf}}(t)$ values plot near the 2.5 Ga crustal evolution line with a few positive values (Supplementary Table S3; Figure 7). These results are similar to those of the 2.2–2.1 Ga granitoids by previous studies [20,28,30,51]. These granitic dykes have low $\text{Mg}^{\#}$ and variable LILE/HFSE ratios (Supplementary Table S1), suggesting that they may have been derived from low-degree partial melting of a thickened crust, rather than subduction of oceanic crust. This magmatic event should have been triggered by delamination-induced extension at the late stage of the orogenic process of the JLJB.

5.3. Implications to the Evolution Model of the JLJB

Although there are matters of debate on the early evolution model of the JLJB, there is a consensus understanding on the orogenic process in Late Paleoproterozoic (e.g., [14,61–64]). The Longgang block and the Liaonan-Nangrim block convergence began at ~2.0 or 1.95 Ga [16,26,65], and widespread metamorphism and deformation are also believed to have taken place at ~1.9 Ga [19,66–69] or ~1.88–1.85 Ga [70,71].

Termination time of the JLJB orogeny was only roughly defined by corresponding granitoids geochronological studies. Garnet-bearing and biotite-bearing porphyritic granites (~1870–1865 Ma), rapakivi granites and alkaline syenite (~1872–1850 Ma) were reported

within the JLJB as products of anorogenic magmatism by previous studies and interpreted as representing the termination of the JLJB orogeny [20,22,72,73]. These geochronological results also met previous metamorphic study results in the JLJB, as ~1.95–1.85 Ga HP and MP granulites in the Jiaobei Block from the Jiaodong Peninsula, the South Liaohe Group in Liaoning Province, and the Ji'an Group in Jilin Province were reported [23,68,69,74,75].

Monzogranitic dykes in this study provide robust constraint on post-collisional granitoids in the JLJB orogeny process. Three granitic dykes observed in this study exhibit manifested post-collisional granite field features by cutting through foliation of the Liaohe Group meta-sedimentary rocks which deformed at ~1.9 Ga by previous studies [23,31,63] (Figure 2). These granitic dykes have transitional features of I- to A-type granites, probably distributing under a post-collisional tectonic setting as [76] illustrated. These monzogranite dykes show features of post-collisional granites in the model proposed by Pearce et al. [59,60] (Figure 8b). Considering these features of the granitoid dykes, the whole-rock geochemistry and Hf isotopic results, we believe these dykes represent exhumation and extension in the final collisional of the orogeny process. The termination collisional time of the JLJB orogen was constrained to be not later than 1860 Ma by these monzogranite dykes.

6. Conclusions

Based on a study of zircon U-Pb geochronology, Hf isotopes and whole-rock geochemistry of the monzogranitic dykes, the following conclusions can be drawn.

- (1) The monzogranite dykes cut through the foliation of the Liaohe Group meta-sedimentary rocks which deformed at ~1900 Ma. Zircons from the monzogranite dyke have euhedral to subhedral shape and high ratio of Th/U, and yield a consistent zircon U-Pb age of ~1859–1852 Ma.
- (2) Two dyke samples have I-type granite and adakitic granite features; the other dyke has a characteristic of A-type granite. Hf isotope data show T_{DM2} ages of 2640–2430 Ma and reveal that most of the $\varepsilon_{Hf}(t)$ values plot near the 2.5 Ga crustal evolution line. Such geochemistry and Hf isotope studies indicate they may have been generated under a delamination of thickened crust tectonic setting.
- (3) The termination collisional time of the JLJB orogen was constrained to be not later than 1860 Ma by these monzogranitic dykes.

Supplementary Materials: The following supporting information can be downloaded at: <https://www.mdpi.com/article/10.3390/min13070928/s1>, Table S1: Major (wt%) and trace ($\times 10^{-6}$) element data for representative samples of the Paleoproterozoic monzogranitic dykes from the Kuandian and Dandong area within the Jiao-Liao-Ji Belt, ($T_{Zr}(^{\circ}C)$: Zircon saturations temperatures by [77]) and ($\delta Eu/Eu^* = Eu N / (Sm N \times Gd N)^{1/2}$, N denotes the chondrite normalization (Sun and McDonough, 1989) [42]). Table S2: LA-ICP-MS zircon U-Pb analyses for representative samples of Paleoproterozoic monzogranitic dykes from the Kuandian and Dandong area within the Jiao-Liao-Ji Belt, Table S3: Lu-Hf isotopic compositions of the in situ zircons of Paleoproterozoic monzogranitic dykes in the Kuandian and Dandong area within the Jiao-Liao-Ji Belt.

Author Contributions: Conceptualization, Y.Z. and X.H.; methodology, P.Z. and J.L.; investigation, Y.Z. and C.C.; writing—original draft preparation, Y.Z.; writing—review and editing, Y.Z., X.H., S.L. and X.Y. All authors have read and agreed to the published version of the manuscript.

Funding: This research was funded by the National Science Foundation of China (Grant No. 42072104; 41502093), Geological Survey Project of China (Grant No. DD20230329; DD20230102), Scientific Research Foundation of Education Department of Liaoning Province (Grant No. LJKQZ20222473, LJKZ1075) and the China Scholarship Council.

Data Availability Statement: Not applicable.

Conflicts of Interest: The authors declare no conflict of interest.

References

1. Zhao, G.C.; Sun, M.; Wilde, S.A.; Li, S.Z. Late Archean to Paleoproterozoic evolution of the North China Craton: Key issues revisited. *Precambrian Res.* **2005**, *136*, 177–202. [[CrossRef](#)]
2. Wilde, S.A.; Zhao, G.C. Archean to Paleoproterozoic evolution of the North China Craton. *J. Asian Earth Sci.* **2005**, *24*, 519–522. [[CrossRef](#)]
3. Zhai, M.G.; Santosh, M. Metallogeny of the North China Craton: Link with secular changes in the evolving Earth. *Gondwana Res.* **2013**, *24*, 275–297. [[CrossRef](#)]
4. Liu, F.L.; Liu, P.H.; Wang, F.; Liu, C.H.; Cai, J. Progresses and overviews of voluminous meta-sedimentary series within the Paleoproterozoic Jiao-Liao-Ji orogenic/mobile belt, North China Craton. *Acta Petrol. Sin.* **2015**, *31*, 2816–2846, (In Chinese with English abstract).
5. Li, S.Z.; Zhao, G.C.; Sun, M.; Han, Z.Z.; Hao, D.F.; Luo, Y.; Xia, X.P. Deformation history of the Paleoproterozoic Liaohe Group in the Eastern Block of the North China Craton. *J. Asian Earth Sci.* **2005**, *24*, 659–674. [[CrossRef](#)]
6. Zhao, G.C.; Cawood, P.A.; Li, S.Z.; Wilde, S.A.; Sun, M.; Zhang, J.; He, Y.H.; Yin, C.Q. Amalgamation of the North China Craton: Key issues and discussion. *Precambrian Res.* **2012**, *222–223*, 55–76. [[CrossRef](#)]
7. Zhang, Q.S.; Yang, Z.S.; Liu, L.D. *Early Crust and Mineral Deposits of Liaodong Peninsula*; Geological Publishing House: Beijing, China, 1988; pp. 218–450, (In Chinese with English abstract).
8. Sun, M.; Armstrong, R.L.; Lambert, R.S.; Jiang, C.C.; Wu, J.H. Petrochemistry and Sr, Pb and Nd isotopic geochemistry of Paleoproterozoic Kuandian Complex, the eastern Liaoning province, China. *Precambrian Res.* **1993**, *62*, 171–190.
9. Bai, J. *The Pre-Cambrian Geology and Pb–Zn Mineralization in the Northern Margin of North China Platform*; Geological Publishing House: Beijing, China, 1993; pp. 47–89. (In Chinese)
10. Li, Z.; Chen, B.; Wei, C.J.; Wang, C.X.; Han, W. Provenance and tectonic setting of the Paleoproterozoic metasedimentary rocks from the Liaohe Group, Jiao–Liao–Ji Belt, North China Craton: Insights from detrital zircon U–Pb geochronology, whole–rock Sm–Nd isotopes, and geochemistry. *J. Asian Earth Sci.* **2015**, *111*, 711–732. [[CrossRef](#)]
11. Li, Z.; Chen, B.; Yan, X.L. The Liaohe Group: An insight into the Paleoproterozoic tectonic evolution of the Jiao-Liao-Ji Belt, North China Craton. *Precambrian Res.* **2019**, *326*, 174–195. [[CrossRef](#)]
12. Li, Z.; Wei, C.J.; Chen, B.; Fu, B.; Gong, M.Y. Late Neoproterozoic reworking of the Mesoproterozoic crustal remnant in northern Liaoning, North China Craton: A U–Pb–Hf–O–Nd perspective. *Gondwana Res.* **2020**, *80*, 350–369. [[CrossRef](#)]
13. Zhu, K.; Liu, Z.H.; Xu, Z.Y.; Wang, X.A.; Cui, W.L.; Hao, Y.J. Petrogenesis and tectonic implications of two types of Liaoji granitoid in the Jiao-Liao-Ji Belt, North China Craton. *Precambrian Res.* **2019**, *331*, 1–19. [[CrossRef](#)]
14. Li, S.Z.; Zhao, G.C.; Santosh, M.; Liu, X.; Dai, L.; Suo, Y.H.; Tam, P.K.; Song, M.; Wang, P.C. Paleoproterozoic structural evolution of the southern segment of the Jiao–Liao–Ji belt, North China Craton. *Precambrian Res.* **2012**, *200–203*, 59–73. [[CrossRef](#)]
15. Zhao, G.C.; Zhai, M.G. Lithotectonic elements of Precambrian basement in the North China Craton: Review and tectonic implications. *Gondwana Res.* **2013**, *23*, 1207–1240. [[CrossRef](#)]
16. Meng, E.; Liu, F.L.; Liu, P.H.; Liu, C.H.; Yang, H.; Wang, F.; Shi, J.R.; Cai, J. Petrogenesis and tectonic significance of Paleoproterozoic meta-mafic rocks from central Liaodong Peninsula, northeast China: Evidence from zircon U–Pb dating and in situ Lu–Hf isotopes, and whole-rock geochemistry. *Precambrian Res.* **2014**, *247*, 92–109. [[CrossRef](#)]
17. Xu, W.; Liu, F.L.; Tian, Z.H.; Liu, L.S.; Ji, L.; Dong, Y.S. Source and petrogenesis of Paleoproterozoic meta-mafic rocks intruding into the North Liaohe Group: Implications for back-arc extension prior to the formation of the Jiao-Liao-Ji Belt, North China Craton. *Precambrian Res.* **2018**, *207*, 66–81. [[CrossRef](#)]
18. Xu, W.; Liu, F.L. Geochronological and geochemical insights into the tectonic evolution of the Paleoproterozoic Jiao–Liao–Ji Belt, Sino-Korean Craton. *Earth Sci. Rev.* **2019**, *193*, 162–198. [[CrossRef](#)]
19. Yang, C.W.; Liu, J.L.; Yang, H.X.; Zhang, C.; Feng, J.; Lu, T.J.; Sun, Y.Q.; Zhang, J. Tectonics of the Paleoproterozoic Jiao-Liao-Ji orogenic belt in the Liaodong peninsula, North China Craton: A review. *J. Asian Earth Sci.* **2019**, *176*, 141–156. [[CrossRef](#)]
20. Liu, F.L.; Liu, C.H.; Itano, K.; Iizuka, T.; Cai, J.; Wang, F. Geochemistry, U–Pb dating, and Lu–Hf isotopes of zircon and monazite of porphyritic granites within the Jiao-Liao-Ji orogenic belt: Implications for petrogenesis and tectonic setting. *Precambrian Res.* **2017**, *300*, 78–106. [[CrossRef](#)]
21. Lu, X.P.; Wu, F.Y.; Guo, J.H.; Yin, C.J. Late Paleoproterozoic granitic magmatism and crustal evolution in the Tonghua region, northeast China. *Acta Petrol. Sin.* **2005**, *21*, 721–736, (In Chinese with English abstract).
22. Yang, J.H.; Wu, F.Y.; Xie, L.W.; Liu, X.M. Petrogenesis and tectonic implications of Kuangdonggou syenites in the Liaodong peninsula, east North China Craton: Constraints from in-situ zircon U–Pb ages and Hf isotopes. *Acta Petrol. Sin.* **2007**, *23*, 263–276, (In Chinese with English abstract).
23. Liu, F.L.; Liu, L.S.; Cai, J.; Liu, P.H.; Wang, F.; Liu, C.H.; Liu, J.H. A widespread Paleoproterozoic partial melting event within the Jiao-Liao-Ji Belt, North China Craton: Zircon U–Pb dating of granitic leucosomes within polydeformed granulites and its tectonic implications. *Precambrian Res.* **2019**, *326*, 155–173. [[CrossRef](#)]
24. Lu, X.P.; Wu, F.Y.; Zhang, Y.B.; Zhao, C.B.; Guo, C.L. Emplacement age and tectonic setting of the Paleoproterozoic Liaoji Granites in Tonghua area, southern Jilin Province. *Acta Petrol. Sin.* **2004**, *20*, 381–392, (In Chinese with English abstract).
25. Yang, H.; Wang, H.; Liu, J.H. Zircon U–Pb dating and its geological significance of granitic pegmatites from the Kuandian and Sanjiazhi area in eastern Liaodong Province. *Acta Petrol. Sin.* **2017**, *33*, 2675–2688, (In Chinese with English abstract).

26. Li, S.Z.; Zhao, G.C. SHRIMP U-Pb zircon geochronology of the Liaoji granitoids: Constraints on the evolution of the Paleoproterozoic Jiao-Liao-Ji belt in the Eastern Block of the North China Craton. *Precambrian Res.* **2007**, *158*, 1–16. [[CrossRef](#)]
27. Wu, F.Y.; Li, Q.L.; Yang, J.H.; Kim, J.N.; Han, R.H. Crustal growth and evolution of the Rangnim Massif, northern Korean Peninsula. *Acta Petrol. Sin.* **2016**, *32*, 2933–3294, (In Chinese with English abstract).
28. Li, Z.; Chen, B.; Wang, J.L. Geochronological framework and geodynamic implications of mafic magmatism in the Liaodong Peninsula and adjacent regions, North China Craton. *Acta Geol. Sin.* **2016**, *90*, 138–153, (In Chinese with English abstract). [[CrossRef](#)]
29. Li, Z.; Chen, B.; Wei, C.J. Is the Paleoproterozoic Jiao-Liao-Ji Belt (North China Craton) a rift? *Int. J. Earth Sci.* **2017**, *106*, 355–375. [[CrossRef](#)]
30. Li, Z.; Li, J.; Chen, B. Early Precambrian tectonic-thermal events: Coupled U-Pb-Hf of detrital zircons from Jiao-Liao-Ji Belt, North China Craton. *Arab. J. Geosci.* **2018**, *11*, 424–440. [[CrossRef](#)]
31. Li, Z.; Meng, E.; Wang, C.Y.; Li, Y.G. Early Precambrian tectono-thermal events in Southern Jilin Province, China: Implications for the evolution of Neoproterozoic to Paleoproterozoic crust in the northeastern North China Craton. *Miner. Petrol.* **2019**, *113*, 185–205. [[CrossRef](#)]
32. Xiao, C.H.; Liu, X.C.; Zhao, Y.; Zhang, Q.; Chen, Z.L.; Liu, J.M.; Wei, C.S.; Yao, X.F.; Wang, W.; Xie, L.Q. Structural controls and Re-Os dating of molybdenite of the Wulong gold deposit, NE China. *Earth Sci.* **2020**, *45*, 3982–3997, (In Chinese with English abstract).
33. Zhao, Y.; Lin, S.F.; Zhang, P.; Yang, X.M.; Gu, Y.C.; Bi, Z.W.; Kou, L.L. Geochronology and Geochemical Characteristics of Paleoproterozoic Syn-orogenic Granitoids and Constraints on the Geological Evolution of the Jiao-Liao-Ji Orogenic Belt, North China Craton. *Precambrian Res.* **2021**, *365*, 106386. [[CrossRef](#)]
34. Chen, J.S.; Xing, D.H.; Liu, M.; Li, B.; Yang, H.; Tian, D.X.; Yang, F.; Wang, Y. Zircon U-Pb chronology and geological significance of felsic volcanic rocks in the Liaohe Group from the Liaoyang area, Liaoning Province. *Acta Petrol. Sin.* **2017**, *33*, 2792–2810, (In Chinese with English abstract).
35. Rudnick, R.L.; Gao, S. Composition of the continental crust. In *The Crust, Treatise in Geochemistry*; Rudnick, R.L., Ed.; Elsevier-Perigamon: Oxford, UK, 2003; Volume 3, pp. 1–64.
36. Liu, Y.S.; Hu, Z.C.; Gao, S.; Günther, D.; Xu, J.; Gao, C.G.; Chen, H.H. In situ analysis of major and trace elements of anhydrous minerals by LA-ICP-MS without applying an internal standard. *Chem. Geol.* **2008**, *257*, 34–43. [[CrossRef](#)]
37. Ludwig, K.R. *Isoplot/Ex, Version 3: A Geochronological Toolkit for Microsoft Excel*; Berkeley Geochronology Centre: Berkeley, CA, USA, 2003.
38. Griffin, W.L.; Pearson, N.J.; Belousova, E.; Jackson, S.E.; Van Ackerbergh, E.; O'Reilly, S.Y.; Shee, S.R. The Hf-isotope composition of cratonic mantle: LAM-MC-ICPMS analysis of zircon megacrysts in kimberlites. *Geochim. Cosmochim. Acta* **2000**, *64*, 133–147. [[CrossRef](#)]
39. Woodhead, J.D.; Hergt, J.M. A preliminary appraisal of seven natural zircon reference materials for in situ Hf-isotope analysis. *Geost. Geoanalytical Res.* **2005**, *29*, 183–195. [[CrossRef](#)]
40. Streckeisen, A.L. Classification of the common igneous rocks by means of their chemical composition: A provisional attempt. *Neues Jahrb. Fur Mineral.* **1976**, *1*, 1–15.
41. Maniar, P.D.; Piccoli, P.M. Tectonic discrimination of granitoids. *Geol. Soc. Am. Bull.* **1989**, *101*, 635–643. [[CrossRef](#)]
42. Sun, S.S.; McDonough, W.F. Chemical and isotopic systematics of oceanic basalts; implications for mantle composition and processes. *Geol. Soc. Lond. Spec. Publ.* **1989**, *42*, 313–345. [[CrossRef](#)]
43. Nowell, G.M.; Kempton, P.D.; Noble, S.R.; Fitton, J.G.; Saunders, A.D.; Mahoney, J.J.; Taylor, R.N. High precision Hf isotope measurements of MORB and OIB by thermal ionisation mass spectrometry: Insights into the depleted mantle. *Chem. Geol.* **1998**, *149*, 211–233. [[CrossRef](#)]
44. Hoskin, P.O.; Schaltegger, U. The composition of zircon and igneous and metamorphic petrogenesis. *Rev. Miner. Geochem.* **2003**, *53*, 27–62. [[CrossRef](#)]
45. Song, Y.H.; Yang, F.C.; Yan, G.L.; Wei, M.H.; Shi, S.S. SHRIMP U-Pb ages and Hf isotopic compositions of Paleoproterozoic granites from the Eastern part of Liaoning Province and their tectonic significance. *Acta Geol. Sin.* **2016**, *90*, 2620–2636, (In Chinese with English abstract).
46. Ren, Y.W.; Wang, H.C.; Kang, J.L.; Chu, H.; Tian, H. Paleoproterozoic magmatic events in the Hupiyu area in Yingkou, Liaoning Province and their geological significance. *Acta Geol. Sin.* **2017**, *91*, 2456–2472, (In Chinese with English abstract).
47. Zhao, Y.; Zhang, P.; Li, Y.; Li, D.T.; Chen, J.; Bi, Z.W. Geochemistry of two types of Paleoproterozoic granites, and zircon U-Pb dating, and Lu-Hf isotopic characteristics in the Kuandian area within the Jiao-Liao-Ji belt: Implications for regional tectonic setting. *Geol. J.* **2020**, *55*, 7564–7580. [[CrossRef](#)]
48. Zhang, P.; Zhao, Y.; Yang, H.Z.; Kou, L.L. Discrimination and its significance of the Sizhanggunzi granite in Kuangdonggou area, eastern Liaoning Province. *J. Northeast. Univ. (Nat. Sci.)* **2016**, *37*, 1349–1352, (In Chinese with English abstract).
49. Yang, M.C.; Chen, B.; Yan, C. Petrological, geochronological, geochemical and Sr-Nd-Hf isotopic constraints on the petrogenesis of the Shuangcha Paleoproterozoic metaporphritic granite in the southern Jilin Province: Tectonic implications. *Acta Petrol. Sin.* **2015**, *31*, 1573–1588, (In Chinese with English abstract).

50. Wang, X.P.; Peng, P.; Wang, C.; Yang, S.Y. Petrogenesis of the 2115 Ma Haicheng mafic sills from the Eastern North China Craton: Implications for an intra-continental rifting. *Gondwana Res.* **2016**, *39*, 347–364. [[CrossRef](#)]
51. Bi, J.H.; Ge, W.C.; Xing, D.H.; Yang, H.; Dong, Y.; Tian, D.X.; Chen, H.J. Paleoproterozoic meta-rhyolite and meta-dacite of the Liaohe Group, Jiao-Liao-Ji Belt, North China Craton: Petrogenesis and implications for tectonic setting. *Precambrian Res.* **2018**, *314*, 306–324. [[CrossRef](#)]
52. Zhao, Y.; Kou, L.L.; Zhang, P.; Bi, Z.W.; Li, D.T.; Chen, C. Characteristics of Geochemistry and Hf isotope from meta-gabbro in the Longchang area, eastern of North China Craton: Implications on the evolution of the Jiao-Liao-Ji Paleoproterozoic orogeny belt. *Earth Sci.* **2019**, *44*, 3333–3345, (In Chinese with English abstract).
53. Wang, X.P.; Peng, P.; Wang, C.; Yang, S.Y. Nature of three episodes of Paleoproterozoic magmatism (2180 Ma, 2115 Ma and 1890 Ma) in the Liaoji belt, North China with implications for tectonic evolution. *Precambrian Res.* **2017**, *298*, 252–267. [[CrossRef](#)]
54. Drummond, M.S.; Defant, M.J. A model for trondhjemite-tonalitedacite genesis and crustal growth via slab melting: Archean to modern comparisons. *J. Geophys. Res. Solid Earth* **1990**, *95*, 21503–21521. [[CrossRef](#)]
55. Whalen, J.B.; Currie, K.L.; Chappell, B.W. A-type granite: Geochemical characteristics, discrimination and petrogenesis. *Contrib. Miner. Petrol.* **1987**, *95*, 407–419. [[CrossRef](#)]
56. Pearce, J.; Harris, N.B.W.; Tindle, A.G. Trace element discrimination diagrams for the tectonic interpretation of granitic rocks. *J. Petrol.* **1984**, *25*, 956–983. [[CrossRef](#)]
57. Pearce, J. Sources and settings of granitic rocks. *Epis. J. Int. Geosci.* **1996**, *19*, 120–125. [[CrossRef](#)]
58. Ma, Y.F.; Liu, Y.J.; Qin, T.; Sun, W.; Zang, Y.Q. Carboniferous granites in the Jalaid Banner area, middle Great Xing’an Range, NE China: Petrogenesis, tectonic background and orogeny accretionary implications. *Acta Petrol. Sin.* **2018**, *34*, 2931–2955.
59. Ma, Y.F.; Liu, Y.J.; Qin, T.; Sun, W.; Zang, Y.Q.; Zhang, Y.J. Late Devonian to early Carboniferous magmatism in the western Songliao–Xilinhot block, NE China: Implications for eastward subduction of the Nenjiang oceanic lithosphere. *Geol. J.* **2020**, *55*, 2208–2231. [[CrossRef](#)]
60. Ma, Y.F.; Liu, Y.J.; Wang, Y.; Qin, T.; Chen, H.J.; Sun, W.; Zang, Y.Q. Late Carboniferous mafic to felsic intrusive rocks in the central Great Xing’an Range, NE China: Petrogenesis and tectonic implications. *Int. J. Earth Sci.* **2020**, *109*, 761–783. [[CrossRef](#)]
61. Zhai, M.G.; Santosh, M. The early Precambrian odyssey of North China Craton: A synoptic overview. *Gondwana Res.* **2011**, *20*, 6–25. [[CrossRef](#)]
62. Liu, P.H.; Liu, F.L.; Yang, H.; Wang, F.; Liu, J.H. Protolith ages and timing of peak and retrograde metamorphism of the high pressure granulites in the Shandong Peninsula, eastern North China Craton. *Geosci. Front.* **2012**, *3*, 923–943. [[CrossRef](#)]
63. Peng, P.; Wang, X.P.; Windley, B.F.; Guo, J.H.; Zhai, M.G.; Li, Y. Spatial distribution of 1950–1800 Ma metamorphic events in the North China Craton: Implications for tectonic subdivision of the craton. *Lithos* **2014**, *202*, 250–266. [[CrossRef](#)]
64. Wu, M.L.; Lin, S.F.; Wan, Y.S.; Gao, J.F. Crustal evolution of the Eastern Block in the North China Craton: Constraints from zircon U–Pb geochronology and Lu–Hf isotopes of the Northern Liaoning Complex. *Precambrian Res.* **2016**, *275*, 35–47. [[CrossRef](#)]
65. Zhou, X.W.; Zhao, G.C.; Wei, C.J.; Geng, Y.S.; Sun, M. Metamorphic evolution and Th–U–Pb zircon and monazite geochronology of high-pressure polytitanic granulites in the Jiaobei massif of the North China Craton. *Am. J. Sci.* **2008**, *308*, 328–350. [[CrossRef](#)]
66. Luo, Y.; Sun, M.; Zhao, G.C.; Li, S.Z.; Xu, P.; Ye, K.; Xia, X.P. LA-ICP-MS U–Pb zircon ages of the Liaohe Group in the Eastern Block of the North China Craton: Constraints on the evolution of the Jiao-Liao-Ji Belt. *Precambrian Res.* **2004**, *134*, 349–371. [[CrossRef](#)]
67. Liou, J.G.; Tsujimori, T.; Chu, W.; Zhang, R.Y.; Wooden, J.L. Protolith and metamorphic ages of the Haiyangsuo Complex, eastern China: A non-UHP exotic tectonic slab in the Sulu ultrahigh-pressure terrane. *Miner. Petrol.* **2006**, *88*, 207–226. [[CrossRef](#)]
68. Tam, P.Y.; Zhao, G.C.; Liu, F.L.; Zhou, X.W.; Sun, M.; Li, S.Z. Timing of metamorphism in the Paleoproterozoic Jiao-Liao-Ji Belt: New SHRIMP U–Pb zircon dating of granulites, gneisses and marbles of the Jiaobei massif in the North China Craton. *Gondwana Res.* **2011**, *19*, 150–162. [[CrossRef](#)]
69. Liu, J.H.; Liu, F.L.; Ding, Z.J.; Liu, C.H.; Yang, H.; Liu, P.H.; Wang, F.; Meng, E. The growth, reworking and metamorphism of early Precambrian crust in the Jiaobei terrane, the North China Craton: Constraints from U–Th–Pb and Lu–Hf isotopic systematics, and REE concentrations of zircon from Archean granitoid gneisses. *Precambrian Res.* **2013**, *224*, 287–303. [[CrossRef](#)]
70. Wan, Y.S.; Song, B.; Liu, D.Y.; Wilde, S.A.; Wu, J.S.; Shi, Y.R.; Yin, X.Y.; Zhou, H.Y. SHRIMP U–Pb zircon geochronology of Paleoproterozoic metasedimentary rocks in the North China Craton: Evidence for a major Late Paleoproterozoic tectonothermal event. *Precambrian Res.* **2006**, *149*, 249–271. [[CrossRef](#)]
71. Meng, E.; Wang, C.Y.; Li, Y.G.; Li, Z.; Yang, H.; Cai, J.; Ji, L.; Ji, M.Q. Zircon U–Pb–Hf isotopic and whole-rock geochemical studies of Paleoproterozoic metasedimentary rocks in the northern segment of the Jiao-Liao-Ji Belt, China: Implications for provenance and regional tectonic evolution. *Precambrian Res.* **2017**, *298*, 472–489. [[CrossRef](#)]
72. Lu, X.P.; Wu, F.Y.; Guo, J.H.; Wilde, S.A.; Yang, J.H.; Liu, X.M.; Zhang, X.O. Zircon U–Pb geochronological constraints on the Paleoproterozoic crustal evolution of the Eastern Block in the North China Craton. *Precambrian Res.* **2006**, *146*, 138–164. [[CrossRef](#)]
73. Liu, J.; Zhang, J.; Liu, Z.H.; Yin, C.Q.; Zhao, C.; Li, Z.; Yang, Z.J.; Dou, S.Y. Geochemical and geochronological study on the Paleoproterozoic rock assemblage of the Xiuyan region: New constraints on an integrated rift-and collision tectonic process involving the evolution of the Jiao-Liao-Ji Belt, North China Craton. *Precambrian Res.* **2018**, *310*, 179–197. [[CrossRef](#)]
74. Liu, J.; Zhang, J.; Liu, Z.H.; Yin, C.Q.; Xu, Z.Y.; Cheng, C.Q.; Zhao, C.; Wang, X. Late Paleoproterozoic crustal thickening of the Jiao-Liao-Ji belt, North China Craton: Insights from ca. 1.95–1.88 Ga syn-collisional adakitic granites. *Precambrian Res.* **2021**, *355*, 106120. [[CrossRef](#)]

75. Yu, H.C.; Liu, J.; He, Z.H.; Liu, Z.H.; Cheng, C.Q.; Hao, Y.J.; Zhao, C.; Zhang, H.Q.; Dong, Y.C. Geochronology and Zircon Hf isotope of the Paleoproterozoic Gaixian Formation in the Southeastern Liaodong Peninsula: Implication for the tectonic evolution of the Jiao-Liao-Ji Belt. *Minerals* **2022**, *2022*, 792. [[CrossRef](#)]
76. Wang, Q.; Mc Dermott, F.; Xu, J.F.; Bellon, H.; Zhu, Y.T. Cenozoic K-rich adakitic volcanic rocks in the Hohxil area, northern Tibet: Lower-crustal melting in an intracontinental setting. *Geology* **2005**, *33*, 465–468. [[CrossRef](#)]
77. Miller, F.H.; McDowell, S.M.; Mapes, R.W. Hot and cold granites? Implications of zircon saturation temperatures and preservation of inheritance. *Geology* **2003**, *31*, 529–532. [[CrossRef](#)]

Disclaimer/Publisher's Note: The statements, opinions and data contained in all publications are solely those of the individual author(s) and contributor(s) and not of MDPI and/or the editor(s). MDPI and/or the editor(s) disclaim responsibility for any injury to people or property resulting from any ideas, methods, instructions or products referred to in the content.